Mechanics of trichocyte alpha-keratin fibers: Experiment, theory, and simulation

Chia-Ching Chou
Laboratory for Atomistic and Molecular Mechanics, Department of Civil and Environmental Engineering, Massachusetts Institute of Technology, Cambridge, MA 02139, USA

Emiliano Lepore
Laboratory of Bio-inspired & Graphene Nanomechanics, Department of Civil, Environmental and Mechanical Engineering, University of Trento, 38123 Trento, Italy

Paola Antonaci
Laboratory of Bio-Inspired Nanomechanics "Giuseppe Maria Pugno", Department of Structural, Geotechnical and Building Engineering, Politecnico di Torino, 10129 Torino, Italy

Nicola Pugno[a),c)]
Laboratory of Bio-inspired & Graphene Nanomechanics, Department of Civil, Environmental and Mechanical Engineering, University of Trento, 38123 Trento, Italy; Center for Materials & Microsystems, Fondazione Bruno Kessler, 38123 Povo (Trento), Italy; and School of Engineering & Materials Science, Queen Mary University of London, London E1 4NS, UK

Markus J. Buehler[b),c)]
Laboratory for Atomistic and Molecular Mechanics, Department of Civil and Environmental Engineering, Massachusetts Institute of Technology, Cambridge, MA 02139, USA

(Received 1 July 2014; accepted 2 September 2014)

The mechanical behavior of human hair is determined by the interaction of trichocyte alpha keratin protein, matrix, and disulfide bonds crosslinking. Much effort has been spent to understand the link between the microscopic structure and the macroscopic fiber properties. Here we apply a mesoscopic coarse-grained model of the keratin macrofilament fibril combined with an analytical solution based on the concept of entropic hyperelasticity of the protein helix to investigate the link between the microscopic structure and the macroscopic properties of keratin fibers. The mesoscopic model provides good agreement with a wide range of experimental results. Based on the mesoscopic model, the predicted stress–strain curve of hair fibers agrees well with our own experimental measurements. The disulfide crosslink between the microfibril–matrix and matrix–matrix contributes to the initial modulus and provides stiffening at larger deformation of the trichocyte keratin fibers. The results show that the disulfide bonds reinforce the macrofilament and enhance the robustness of the macrofilament by facilitating the microfilaments to deform cooperatively. The availability of a mesoscopic model of this protein opens the possibility to further explore the relationship between microscopic chemical structure and macroscopic performance for a bottom-up description of soft materials.

I. INTRODUCTION

Hair fiber is a hierarchical structure ranging from alpha-helix, coiled-coils, microfibrils, macrofibrils to fibers, as sketched in Fig. 1(a). The primary structural molecules in wool and hair fibers are keratin intermediate filament (IF) proteins, forming a microfibril which is built from the assembly of coiled-coils (heterodimers). The IF is embedded in a sulfur-rich protein matrix and assembles into macrofibrils. For keratinized materials, the elastic modulus ranges from approximately 1–4 GPa. Specifically, the modulus is 1.6–4.5 GPa[1,2] in wool, 2.0–3.7 GPa[3–5] in human hair, 1.0–3.5 GPa[2] in porcupine quill, and 0.4 GPa[2,6] in hoof.

Fueled by demand from the textile industry, intensive studies have examined this class of proteins from the 1930s onwards,[7–11] aiming at explaining the mechanical behavior of keratin-based fibers and the link between the structural change and the mechanical properties. As a result of experimental work, several deformation models were proposed to interpret the shape of stress–strain curves, and to correlate with the fiber structure to explain the mechanical behavior of keratin fibers.[12–21] Earlier deformation mechanism models were proposed by

Address all correspondence to these authors.
[a)]e-mail: nicola.pugno@unitn.it
[b)]e-mail: mbuehler@MIT.EDU
[c)]These authors were editors of this focus issue during the review and decision stage. For the *JMR* policy on review and publication of manuscripts authored by editors, please refer to http://www.mrs.org/jmr-editor-manuscripts/.
DOI: 10.1557/jmr.2014.267

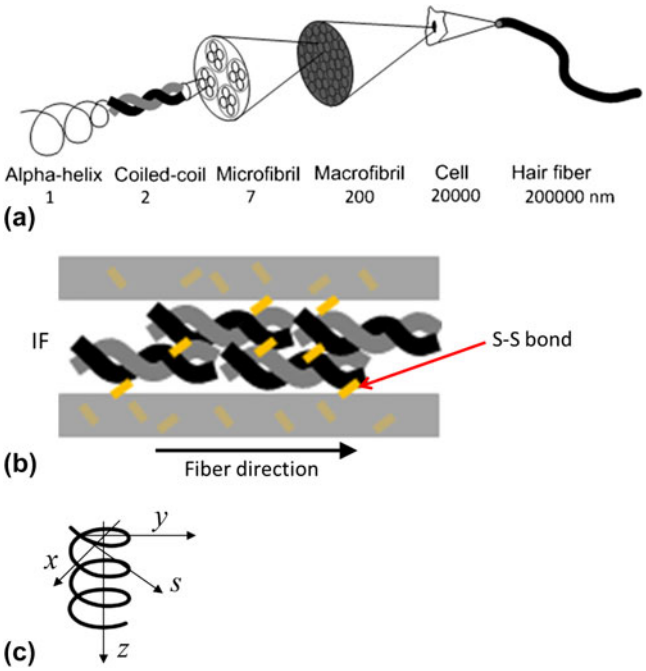

FIG. 1. (a) Human hair features a hierarchical structure, ranging from alpha-helix, dimers with a coiled-coil structure, microfibrils, macrofibrils to the cellular structure, and eventually entire hair fiber level. (b) Schematic visualization that shows IFs are embedded in the matrix connected by intramolecular disulfide bonds (S–S bond in the figure). (c) Geometry of the coil and reference system.

Hearle[12–14] and Feughelman.[15–19] The deformation models used to describe the mechanical behavior of keratin fiber focus primarily on the geometric change of microfibril/matrix structure. In this earlier work, the authors attempted to interpret the shape of curve in relation to the keratin IF protein (coiled coil structure) and an amorphous matrix structure. The major difference between these two models is that the Feughelman model does not take into account any interaction between the coiled coil region and the matrix, while the model proposed by Chapman and Hearle does. Besides these deformation models, previous computational studies of keratin proteins and other α-helical proteins, such as vimentin IF, focusing on the atomistic configuration and nanomechanical properties at atomistic scale have been reported.[22–27] However, relatively little is known of the physical mechanisms that drive its deformation behavior, thus presenting an opportunity to generate a new approach that considers the structure–property paradigm from the atomistic level to the macroscopic scale. To provide a bottom-up description of materials behavior from a fundamental perspective, here we apply a multiscale simulation approach that links the molecule's chemical structure (including the abundance of disulfide cross-links) and its larger-scale properties. Using the multiscale simulation, we are able to upscale the atomistic simulations based on the architecture of materials to exploit insights that are relevant for bioengineering and other applications.

The study reported in this paper is aimed to build a mesoscopic simulation model of keratin macrofilaments and to link the microscale structural changes with the stress–strain curves of large-scale keratin fibers. We demonstrate that the deformation prediction from the mesoscopic model is in good agreement with the stress–strain curve in experiments, and it provides insights and a general methodology to assess the mechanics of other biological systems.

II. MATERIALS AND METHODS

A. Samples

Samples were randomly taken from a 39-year-old male donor and a 36-year-old female donor. Both pigmented (AC) and white (AW) male hairs belong to the same individual – age 39. Both pigmented (PC) and white (PW) female hairs belong to the same individual – age 36. The geometrical parameters of the hair samples are listed in Table I.

B. Tensile testing setup

The hair ends were cut off to isolate a central portion of about 60–70 mm. Then each sample edge was provided with a knot and subsequently glued to a cardboard support, resulting in a final net length as reported above. Testing apparatus is MTS Insight electrochemical testing system – 1 kN – standard length. Tensile test is in displacement control. The load is applied up to specimen failure. The loading rate is 10 mm/min.

C. Mesoscale modeling

In this study, a mesoscopic "bead-spring" method is used to investigate the mechanics of trichocyte keratin macrofilament with disulfide crosslinks. The method is a coarse-grained description of alpha-helical protein and matrix structure. This has proven to be a suitable approach to simulate certain aspects of alpha-helix based proteins, such as intermediate filaments in the cell's cytoskeleton[28,29] and other fibril protein systems, such as collagen fibril with mineral and various cross-link densities.[30–32] In the mesoscale model, each bead represents clusters of amino acids in explicit solvent, and all of beads interact according to a specific intermolecular multibody potential to reflect the physical behavior of keratin proteins. The total energy of the interaction of beads in the system, E_{tot}, is expressed as

$$E_{\text{tot}} = E_{\text{bond}} + E_{\text{angle}} + E_{\text{nonbonded}} \quad , \qquad (1)$$

where E_{bond} is the bonded interaction describing the stretching behavior, E_{angle} is the bending energy, and $E_{\text{nonbonded}}$ is the nonbonded energy due to the van der Waals interactions. Within each intermediate filament,

TABLE I. Overview of experimental specimens.

	AC series			AW series		PC series		PW series		
Specimen description	Pigmented male hair [a]			White male hair [a]		Pigmented female hair [b]		White female hair [b]		
Number of specimens	10			10		10		10		
Diameter [c] (m)	68.60			71.82		61.55		78.08		
Length [d] (mm)	AC01	AC02	AC03	AC04	AC05	AC06	AC07	AC08	AC09	AC10
	39.1	38.2	43.2	37.2	41.9	44.4	46.2	33.6	45.6	36.2
	AW01	AW02	AW03	AW04	AW05	AW06	AW07	AW08	AW09	AW10
	33.6	34.5	42.5	34.7	34.3	42.2	35.7	45.1	31.8	35.9
	PC01	PC02	PC03	PC04	PC05	PC06	PC07	PC08	PC09	PC10
	40.0	48.3	36.8	38.8	45.2	32.5	46.4	44.1	43.2	43.5
	PW01	PW02	PW03	PW04	PW05	PW06	PW07	PW08	PW09	PW10
	32.3	32.1	30.1	31.8	30.9	33.9	31.7	38.8	33.1	34.4

[a]Both pigmented and white male hairs belong to the same individual – age 39.
[b]Both pigmented and white female hairs belong to the same individual – age 36.
[c]Mean value over 18 measurements, performed on 3 hairs per series, using SEM.
[d]The specified values refer to net lengths, after sample preparation for test.

a multilinear model provides a nonlinear force-extension behavior of intermediate filament under stretching as

$$F(r) = -\frac{\partial E_{\text{bond}}(r)}{\partial r} = \begin{cases} k_1(r - r_0) & r<r_1 \\ k_1(r_1 - r_0) + k_2(r - r_1) & r_1<r<r_2 \\ k_1(r_1 - r_0) + k_2(r_2 - r_1) + k_3(r - r_2) & r_2<r<r_3 \\ k_1(r_1 - r_0) + k_2(r_2 - r_1) + k_3(r_3 - r_2) + k_4(r - r_4) & r_3<r<r_4 \\ 0, & r_4<r \end{cases}, \quad (2)$$

where $F(r)$ is the force between two beads, and k_1, k_2, k_3, k_4 are four spring constants which represent the stiffness of molecular stretching at different regimes as shown in Fig. 2(a)-(d). The force displacement relationship in Eq. (2) is fitted to reproduce the nanomechanical behavior obtained using the full atomistic model of keratin tetramer[25] which has been well validated against experimental measurements. $E_{\text{angle}} = \frac{1}{2}k_\theta(\theta - \theta_0)^2$ with $k_\theta = \frac{3EI}{r_0}$, where EI is the bending stiffness, and θ is the angle between three beads relative to the equilibrium angle, θ_0. The bending stiffness, EI, can be obtained through the relationship of $EI = L_p k_B T$, where L_p is the intermediate filament persistence length, k_B is the Boltzmann constant, and T is the temperature. The bending stiffness, EI, is obtained from bending deformation calculations of alpha-helical molecules in the previous publications.[33,34] The nonbonded interaction, $E_{\text{nonbonded}}$, is described by Lennard–Jones potential to simulate the van der Waals interactions between the filament chains and matrix-filament, $\phi_{LJ} = 4\varepsilon\left[\left(\frac{\sigma}{r}\right)^{12} - \left(\frac{\sigma}{r}\right)^{6}\right]$, where ε is the energy at equilibrium and σ is the distance as $\phi_{LJ} = 0$. A harmonic/shift/cut function in LAMMPS[35] with spring stiffness of 7.35 kcal/mol/Å^2 is applied to model the disulfide crosslinking. When the bond deformation is larger than 4 Å, the disulfide crosslinking breaks and the force drops to zero. The parameters are based on the full atomistic simulation results using ReaxFF reactive force field.[36] The time step used in our coarse-grained model is 20 fs. The simulations are performed using the large-scale atomic/molecular massively parallel simulator (LAMMPS).[35] The mesoscopic parameters of the coarse-grained trichocyte keratin macrofilament model are summarized in Table II.

In the coarse-grained model, the full length sequence of tetramer is replaced by a chain of beads, and eight chains of the tetramer model are placed in a cylinder with diameter 7.0 nm to form a microfilament according to the measurement using x-ray scattering on human hair.[37,38] The filaments are placed on a hexagonal lattice packing based on the observation in experiments shown in Fig. 2(b).[39] The distance between the center of mass of one filament and its nearest neighbor is determined by the experimental mean filament–filament distance 9.0 nm.[37,38] Assuming that the eight chains are close packed on the cylinder, the diameter of one filament particle is roughly equal to the one-eighth of the circumference of the cylinder. Since a keratin tetramer is ~50 nm long and has a molecular weight of 200 kg/mol (around 2000 amino acids), one filament bead represents about 60 amino acids with a molecular weight of

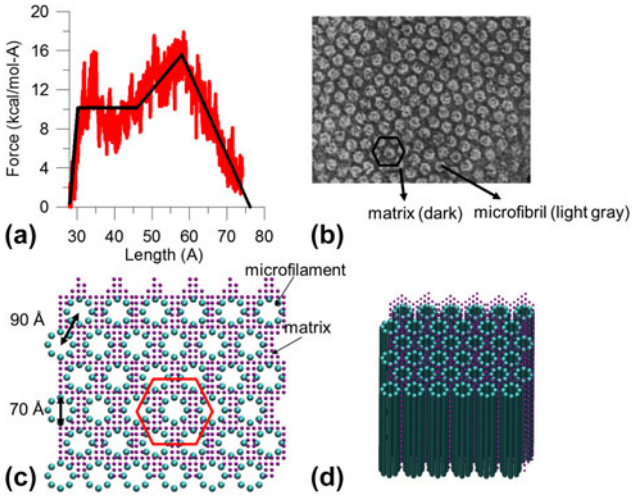

FIG. 2. (a) The force–strain relationship of individual keratin microfilament in our bead-spring model is derived from full-atomistic simulations[25] and has been validated against experimental studies. (b) Electron micrograph of the central portion of macrofibril in the cortex of fine wool depicts the hexagonal microfibril packing in macrofibril.[39] Reprinted from Journal of Structural Biology, Vol. 142(2), R.D. Bruce Fraser and D.A.D. Parry, Macrofibril assembly in trichocyte (hard α-) keratins, Copyright (2003), with permission from Elsevier. (c, d) Coarse-grained model of keratin macrofibril. The filaments are placed on a hexagonal lattice.

TABLE II. Summary of the parameters used in the mesoscopic model.

Parameter and units	Numerical value
Equilibrium bead distance r_0 (Å)	28
Critical distances r_1, r_2, r_3, r_4 (Å)	30.257, 45.96, 57.93, 75.6
Tensile stiffness parameters k_1, k_2, k_3, k_4 (kcal/mol/Å^2)	4.49, 0.0, 0.46, −0.86
Equilibrium angle θ_0 (°)	180
Bending stiffness parameter k_θ (kcal/mol/rad^2)	3.44
Equilibrium energy ε (kcal/mol)	6.8
Equilibrium distance σ (Å)	25

12 kg/mol. The diameter of the matrix is determined using the separation between two filaments to place at least one particle between the filaments. Based on all of the structural parameters and the molecular weight fraction of microfibrils (43%) and matrix (28%) in experiments,[39] we calculate the ratio of the number of filament and matrix beads equal to 12. Finally, the coarse-grained model containing the microfilaments embedded in the matrix is shown in Fig. 2(c).

D. Mechanical analysis in the simulation

Pulling is applied in fiber-direction to model a tensile loading, as indicated in Fig. 1(b). We stretch the systems by deforming the simulation box length in the fiber-direction. In this study, we choose a small strain rate of 0.01 m/s which is computationally feasible, and no major rate effect on the system is observed. The simulations are carried out at 300 K in an NVT ensemble (constant temperature, constant volume, and constant number of particles). During the simulation, the pressure in fiber-direction and the box length are monitored to measure the stress–strain curve. The strain is defined by $\varepsilon = \frac{\Delta L}{L}$ (= engineering strain), where ΔL is the applied elongation and L is the length of the system in the pulling direction. The initial elastic modulus (Young's modulus) is calculated as the steepest slope of the stress–strain curve in the initial linear region.

E. Entropic hyperelasticity of helix

1. Hyperelasticity

Here, we use an entropic hyperelasticity of helix model to describe the behavior of alpha-helix domain in hair. The coil geometry shown in Fig. 1(c) is described by the following equations:

$$x = r\cos 2\pi\frac{s}{l} \quad , \tag{3}$$

$$y = r\sin 2\pi\frac{s}{l} \quad , \tag{4}$$

$$z = \lambda\frac{s}{l} \quad , \tag{5}$$

where r is the radius of the coil, s is the curvilinear coordinate, l is the length of a ring, and λ is the distance between two adjacent rings. The coil angle is defined by $\tan\alpha = \frac{\lambda}{2\pi r}$.

If two self-equilibrated forces F are applied along z at the ends of the coil, its elastic energy per unit length will be

$$\frac{dE_L}{ds} = \frac{1}{2}\left(\frac{N^2}{EA} + \frac{M^2}{GI_p}\right) \quad , \tag{6}$$

where N is the axial load, M is the twisting moment, E and G are the material Young and shear modulus, A is the cross-section area, and I_p is the torsional (e.g., polar, for circular cross-sections) moment of inertia of the fiber. It is worth noting that $M = Fr$, $N = F\sin\alpha$, we can easily derive the elastic energy in the coil composed by m rings, as

$$E_L = \frac{m}{2}\frac{F^2}{EA}\left(\sin^2\alpha + 2(1+\nu)\frac{Ar^2}{I_p}\right)l \quad , \tag{7}$$

where v is the Poisson's ratio. The equivalent (in terms of stored energy) elastic stiffness can be derived by comparison with

$$E_L = \frac{1}{2}\frac{F^2}{K_E} \quad , \tag{8}$$

yielding

$$K_{\mathrm{E}} = \frac{EA/ml}{\sin^2\alpha + 2(1+\nu)\frac{Ar^2}{I_{\mathrm{p}}}} \quad . \tag{9}$$

Note that $\frac{Ar^2}{I_{\mathrm{p}}}$ describes the slenderness of a ring and $\frac{EA}{l}$ its axial stiffness.

Now we consider the actual values of r and α as imposed by a nominal strain $\varepsilon = \frac{\lambda-\lambda_0}{\lambda_0}$, where subscript 0 refers to the unstrained initial configuration. The strained coil geometry, described by the two functions $\alpha(\varepsilon)$ and $r(\varepsilon)$, can be deduced by imposing the inextensibility of the coil (i.e., neglecting the axial compliance with respect to the torsional one), i.e., imposing $l = l_0$, from which we obtain

$$\sin\alpha(\varepsilon) = \sin\alpha_0(1+\varepsilon) \quad , \tag{10}$$

and then consequently

$$r(\varepsilon) = r_0\frac{\cos\alpha(\varepsilon)}{\cos\alpha_0} = r_0\sqrt{1-\frac{\varepsilon^2+2\varepsilon}{\frac{1}{\sin^2\alpha_0}-1}} \quad . \tag{11}$$

The coil will reach the straight configuration ($\sin\alpha(\varepsilon^*) = 1$) under a critical strain

$$\varepsilon^* = \frac{l-\lambda_0}{\lambda_0} = \frac{1}{\sin\alpha_0} - 1 \quad . \tag{12}$$

Thus, in general, the hyperelastic stiffness of a coil of contour length ml per cross-section area can be described by

$$K_{\mathrm{HE}}(\varepsilon) = K_{\mathrm{E}}A\lambda_0 = \begin{cases} \dfrac{E\lambda_0/ml}{\sin^2\alpha_0(1+\varepsilon)^2+2(1+\nu)\frac{A}{I_{\mathrm{p}}}r_0^2\left(1-\frac{\varepsilon^2+2\varepsilon}{\frac{1}{\sin^2\alpha_0}-1}\right)}, & \varepsilon<\varepsilon^* \\ \dfrac{E\lambda_0}{ml}, & \varepsilon\geq\varepsilon^* \end{cases} . \tag{13}$$

2. Hydrogen bonds (H-bonds)

We describe a stiffness of a linear elastic spring with a bundle of H-bonds between two adjacent coils as K_{HB}. We estimate the value of K_{HB} from the MD simulation results,[40,41] where the 3.6 H-bonds in one convolution break simultaneously, and the corresponding energy barrier and the distance between the equilibrated state and the transition state are $E_{\mathrm{HB}} = 11.1$ kcal/mol and $\Delta b_{\mathrm{HB}} = 1.2$ Å. Thus, K_{HB} can be obtained by

$$K_{\mathrm{HB}} = \frac{(E_{\mathrm{HB}}/\Delta b_{\mathrm{HB}})N}{A} \quad , \tag{14}$$

where N is the number of alpha-helices in an unit area A. We apply the cross-section area ~10 nm^2 (Ref. 42) of a tetramer that consists of 4 alpha-helices, and we obtain $K_{\mathrm{HB}} = 254.8$ MPa.

It is worth noting here that for alpha-helical structure, the previous studies have shown that the hydrophobic interactions between helices have relatively small contribution.[43] Also, in trichocyte keratins, the full atomistic model showed that the disulfide bonds hinder the sliding behavior between coils[25] so that there is little contribution of interaction between helices to the force. Thus, the interaction between helices including hydrophobic interaction is not considered in our theoretical model.

III. RESULTS AND DISCUSSION

In this study, we consider three different approaches to identify how the trichocyte keratin fiber with disulfide crosslink responds to mechanical deformation. First, tensile tests of hair samples in experiments. Second, a mesoscopic model of keratin macrofilament with disulfide crosslink. Finally, we report a force–displacement relationship based on the helix-like theoretical model.

A series of tensile tests are performed on all the different hair samples. The results of stress–strain curves are shown in Fig. 3. Mean values of failure stress, failure strain, Young's modulus, and toughness for the different hair samples are depicted in Fig. 4. The results clearly show that the stress–strain curves of keratin fibers share a high level of similarity, and that there is almost no significant difference in the mechanical properties between different hair samples. The stress–strain curve of keratin fibers, as shown in Fig. 3, features a characteristic shape that can be divided into three different regimes based on the profile of the curve and the varied physical phenomena related to each regime. The results are similar to the ones reported in the literature. In the first regime, from 0 to ~4% strain, the stress increases linearly with strain displaying an elastic behavior. In the second regime, from 4 to ~20% strain, the stress reaches a plateau regime where the stress remains almost constant. It is found that the unfolding of alpha-helical domains and a transition of alpha-helical to beta-sheet structure occur in this regime. In the last regime (strain >20%), the stress increases again as the strain increases. The increased stiffness is caused by the stretching of covalent bonds of the protein backbone.

To further understand how the trichocyte keratin materials respond under an external force, it is important to develop a model which reflects the composite structure of keratin materials and allows us to probe the effect of disulfide crosslinks. Since the experiments suggest that macrofilament serves as the major component of trichocyte keratin,[39] we build a mesoscopic model of the macrofilament consisting of microfilaments and matrix with disulfide crosslinks inside the matrix and in between the matrix

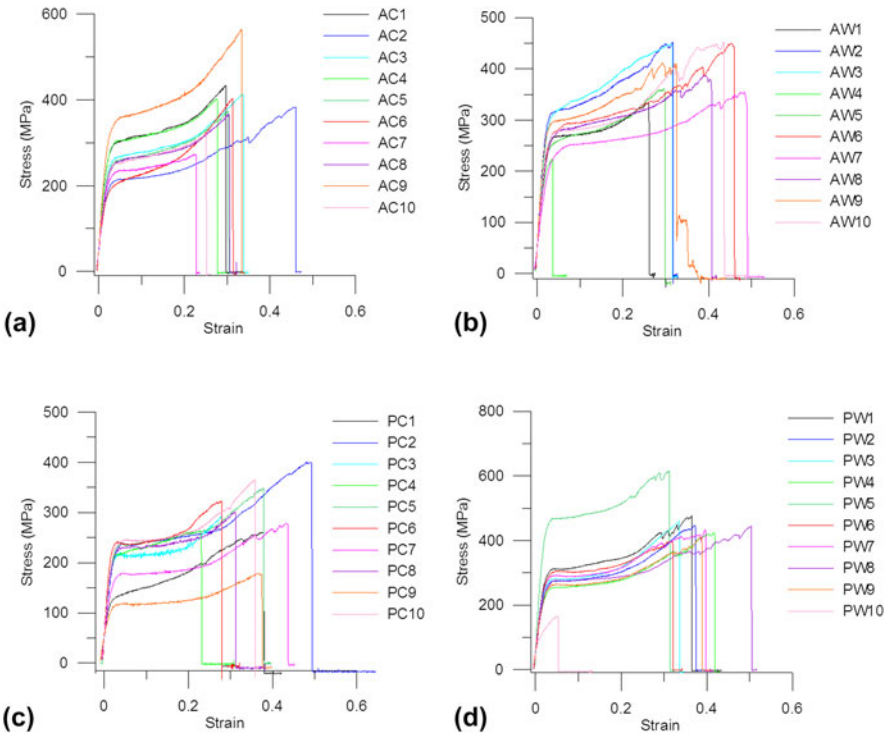

FIG. 3. Tensile stress–strain curves of (a) pigmented male hair (AC), (b) white male hair (AW), (c) pigmented female hair (PC), and (d) white female hair (PW).

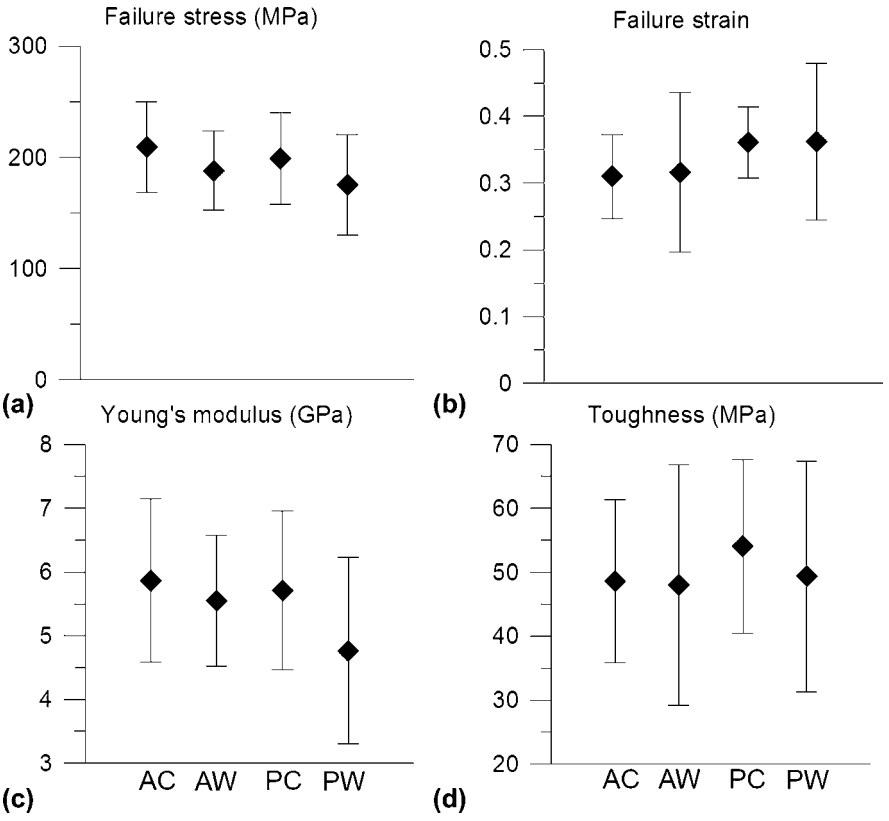

FIG. 4. Mechanical properties of AC, AW, PC, and PW under external tensile loading. (a) Failure stress, (b) Failure strain, (c) Young's modulus, and (d) Toughness.

and the microfilament as shown in Figs. 2(c) and 2(d). Details about the model formulation are included in the Materials and Methods section.

We proceed with stretching the systems by deforming the simulation box length in fiber-direction and measure the stress–strain response of this material, until failure occurs. Figure 5(a) depicts stress–strain curves of the mesoscopic macrofilament model. We observe three major regimes in the stress–strain response. In the first regime (I), the stress increases linearly under a small deformation (strain <7%). In the second regime (II), a relative flat increase in stress from 7 to 17% strain, followed by an increasing stiffness of the stress, which lasts up to the stress close to 80 MPa (III). Eventually, strong bonds in the microfilaments chains break, and the entire system fails at 30% strain. The phenomenon of the increase of the stress in the regime (III) is referred to as strain hardening.

The stress–strain curves of the mesoscopic simulation feature the similar characteristic shape as the experimental measurements. From the analysis of the stress–strain behavior, the Young's modulus = 1.38 GPa is calculated as the steepest slope of the stress–strain curve in the region (I). This modulus is close to experimental results for human hair, where a range of 1.1[44] to 6 GPa (our experiments) was reported.[45] The maximum strain for the mesoscopic filament model is predicted to be 30% [Fig. 5(a)] which is close to experimental measurements of ~33%. We note that the maximum stress, 80 MPa, of our mesoscopic model is almost twice smaller than the experimental data. The discrepancies between the experiments and the simulation might be caused by the fact that whole hair samples are considered in experiment, whereas a part of macrofilament system without any structural flaws is modeled in our simulations.

We further analyze the disulfide crosslink responses during the pulling. Figure 5(b) depicts the decrease of disulfide crosslink content which is normalized by the number of disulfide bonds in the initial model plotted as a function of increasing applied strain. This plot also exhibits three different regimes during mechanical strain. The rupture of disulfide bonds occurs from the start of straining (0–7%). This shows the rupture of the linkages between the matrix and the IFs, and the results further support Chapman's and Hearle's model that incorporates a link between the matrix and the IFs. In the second regime, the curve shows a small decrease in the crosslink content until ~17% strain, followed by a rapid decrease again until the system fractures. This phenomenon is consistent to the experimental measurement using Raman spectra.[45] Figure 5(c) shows the simulation snapshots of the macrofilament at different applied strains. Under strain, the microfilaments deform cooperatively, and the chains start aligning along the fiber direction. At the larger strain, once a bundle of the microfilaments breaks, the system fails. The coarse-grained model is developed from a bottom-up approach and parameterized from the previous full atomistic study[25] so we expect that the stress–strain curve of the coarse-grained simulation

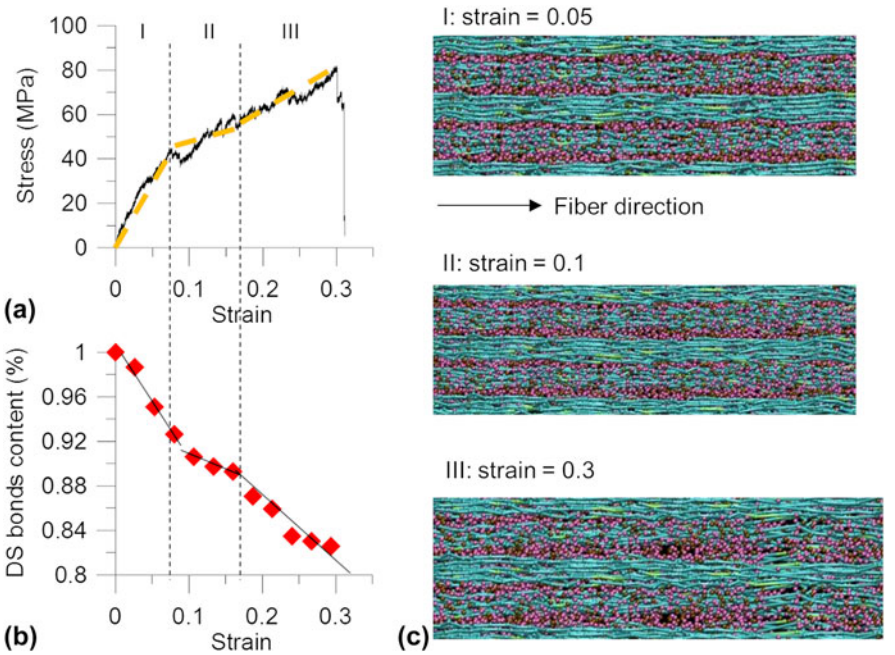

FIG. 5. (a) The stress–strain curves of coarse-grained simulation. (b) Decrease of disulfide crosslink content, normalized by the number of disulfide bonds in the initial model. (c) Simulation snapshots at different pulling strains.

and the experiments [Fig. 3] might not perfectly match. However, despite its simplicity, our model captures the essential physical properties of alpha-helical based keratin macrofilaments as identified in earlier theoretical and experimental studies. Through simulation of a larger-scale filament and matrix structure, our model enables us to provide an important link between single molecule properties and mechanisms and the overall material behavior at much larger length-scales.

We proceed with the study of mathematical equation of hyperelastic stiffness coil model linking the structural change and stress–strain curve of keratin fiber through a spring model. Under small deformation, the stretch of H-bonds in convolutions of alpha-helical structure in keratin proteins plays the major role. The stiffness of an alpha-helix can be calculated as [H-bonds in parallel to the elasticity of a coil as plotted in Fig. 6(a)]

$$K = K_{\mathrm{HB}} + K_{\mathrm{HE}} \quad . \tag{15}$$

Once the deformation of H-bonds elongates to a critical point Δb_{HB} which is the critical displacement for H-bond fracture, the unfolding of alpha-helix occurs. We consider a chain with N units of folded structure involved in H-bond fracture and assume that the ratio of units of folded structure is $\frac{Nx_\alpha}{L(N)} = \frac{Nx_\alpha}{(L_0+Nx_\alpha)} = 0.15$, where $L(N)$ is the total length of the chain, L_0 is the length of chains not involved in H-bond fracture, and x_α is the unit length of helix. Thus, due to $\frac{\Delta b_{\mathrm{HB}}}{x_\alpha} = \frac{1.2}{5.4} = 0.22$, the critical strain for the rupture of H-bonds $\varepsilon_1 = \frac{N\Delta b_{\mathrm{HB}}}{(L_0+Nx_\alpha)} = 0.03$ can be obtained. Beyond the critical point ε_1, the helical structures start to unfold, and the regime is dominated by the hyperelasticity mechanics until the coil reaches the straight configuration where the backbone of the protein starts to be stretched at the strain ε^* in Eq. 13. It is known that the ratio of the unit length of helix (x_α) to its contour length (λ) is about 0.5, i.e., $\varepsilon^* = \frac{\lambda - x_\alpha}{2x_\alpha} \approx 1.0$; based on the previous atomistic simulation,[22] assuming the ratio of the length of helix structure (Mx_α) involved in the unfolding $\frac{Mx_\alpha}{L(N)} = \frac{Mx_\alpha}{(L_1+Mx_\alpha)} \approx 0.4$, where L_1 is the length of chains not involved in unfolding, the critical strain for the alpha-helix unfolding is $\varepsilon_2 = \frac{M(\lambda - x_\alpha)}{(L_1+Mx_\alpha)} = 0.4$. After the hyperelasticity regime where $\varepsilon < \varepsilon_2$, the intrinsic axial stiffness of the fiber, $K_{\mathrm{HE}} = \frac{E\lambda_0}{ml}$, dominates up to fracture.

Here we further apply a binomial distribution to consider the effect of disulphide crosslinks in the system. We assume that the number of breaking disulfide bonds is k, each with a bond breaking probability p. The total number of disulfide bonds is n so that the probability of k bonds breaking in a pulling event is given by a binomial distribution:

$$b = \binom{n}{k} p^k (1-p)^{n-k} \quad . \tag{16}$$

Moreover, we assume that after a certain number x of disulfide bonds are broken, the system fails. The probability that the total number X of disulfide bonds breaking, with a given probability distribution b, during the entire pulling process will exceed the tolerance x is given by

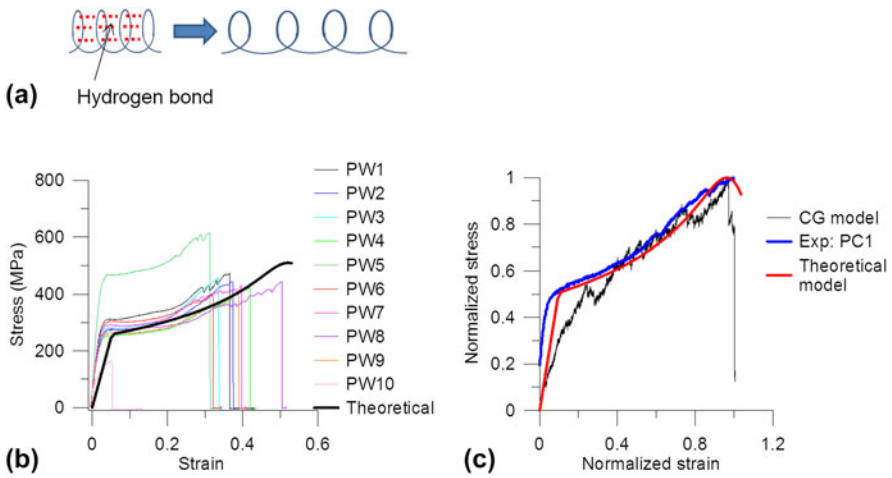

FIG. 6. (a) Illustration of H-bonds in parallel in coils and unfolding of the helical structures. (b) Comparison of stress–strain curves of experimental data and theoretical prediction based on the stiffness in Eq. (18), where the parameters in binomial distribution are obtained by fitting the failure stress, failure strain and the critical point at onset of the third regime in stress–strain curves of keratin fibers. (c) Comparison of normalized stress–strain curves of coarse-grained simulation, theoretical prediction, and experimental data. The stress and strain are normalized to the maximum values in each data set, individually, to compare the shape of stress–strain curves and the mechanical response in tensile testing. The raw data of stress–strain curves for experimental data, CG simulation, and theoretical formulation are shown in Figs. 3(c), 5(a), and 6(b) separately.

$$B = 1 - \sum_{i=0}^{x} \binom{n}{i} p^i (1-p)^{n-i} \quad . \tag{17}$$

The parameters used in the binomial distribution are obtained by fitting the failure stress, failure strain and the critical point at the onset of the third regime in the experimental stress–strain curves of keratin fibers. The fitted binomial distribution mainly affects the third regime of the stress–strain curve but has little effect below the critical point at the onset of the third regime. Thus, considering the breaking of disulfide bond under stretching, the stiffness of an alpha-helical chain can be described by

$$K = B(K_{\mathrm{HE}} + K_{\mathrm{HB}}) \quad . \tag{18}$$

Based on the stiffness in Eq. (18), the stress–strain relationship is given by $\sigma = K\varepsilon$, where σ is the stress and ε is the engineering strain. Figure 6(b) depicts the comparison of the stress–strain curve of the theoretical model and experiments. The result shows that the theoretical data agrees well with the experiments as the value of the stress–strain curves of the theoretical data is within the range of the experimental data set. The availability of a theoretical model of the helix provides a mathematical equation as a basis to explore the relationship between structure, mechanical properties and performance from a theoretical perspective. The good agreement between the results of experimental data and theoretical formulation suggests that the behavior of helix domain plays a dominant role in hair as stated in literature.[14,18] We also compare the mesoscale simulation results with experimental data and theoretical prediction plotted in Fig. 6(c). The stress and strain are normalized to the maximum values in each data set, individually, to compare the shape of stress–strain curves and the mechanical response in tensile testing. The comparison in Fig. 6(c) shows that the stress–strain curves have similar shape which features three regimes. In the first regime (I), both stresses increase linearly with strain. In the second (II), a stress plateau relates to the unfolding of the coiled-coil segments and alpha-helical structure. For the third (III) regime, the stretching of the backbone of the alpha-helix with the breaking of disulfide crosslinks causes the strain stiffening of the material, and the system fails.

IV. CONCLUSION

The study reported here presented a mesoscopic coarse-grained model to link the microscopic structure of trichocyte keratin fibers to the mechanical properties at larger scales. The composite structure of keratin fiber at the mesoscale is addressed using a bead-spring model for a keratin macrofilament. Mesoscale beads represent coiled-coil keratin tetramer proteins which are assembled to filaments and embedded in a matrix of soft particles with disulfide crosslinks. The mesoscopic model gives good agreement with a wide range of experimental results. The stress–strain curve of hair fibers predicted by the mesoscopic model agrees well with our experimental data. The disulfide crosslink between the microfibril–matrix and matrix–matrix contributes the initial modulus and provides stiffening at larger deformation of trichocyte keratins. The results show that the disulfide bonds reinforce the macrofilament and enhance its robustness by facilitating the microfilaments to deform cooperatively. The availability of the coarse-grained multiscale model now allows us to study the mechanical properties at larger scales of keratin fibrils, and perhaps entire hair fibers. The mesoscopic model of keratin fiber built here could be directly extended to other soft fibrous-matrix materials, such as porcupine quills.

ACKNOWLEDGMENTS

Chia-Ching Chou and Markus J. Buehler acknowledge funding from AFOSR whereas Nicola M. Pugno is supported by the European Research Council (ERC StG Ideas 2011 BIHSNAM n. 279985 on “Bio-Inspired hierarchical super-nanomaterials”, ERC PoC 2013-1 REPLICA2 n. 619448 on “Large-area replication of biological anti-adhesive nanosurfaces”, ERC PoC 2013-2 KNOTOUGH n. 632277 on “Super-tough knotted fibres”), by the European Commission under the Graphene Flagship (WP10 “Nanocomposites”, n. 604391) and by the Provincia Autonoma di Trento (“Graphene Nanocomposites”, n. S116/2012-242637 and reg.delib. n. 2266).

REFERENCES

1. W. Oxenham: The mechanics of wool structures R. Postle, G.A. Carnaby, and S. de Jong, Ellis Horwood, Chichester, 1988. pp. 462, price £59.50. ISBN 0-7458-0322-9. *Br. Polym. J.* **21**(3), 279 (1989).
2. S.F. Chou and R.A. Overfelt: Tensile deformation and failure of North American porcupine quills. *Mater. Sci. Eng., C* **31**(8), 1729 (2011).
3. I.P. Seshadri and B. Bhushan: In situ tensile deformation characterization of human hair with atomic force microscopy. *Acta Mater.* **56**(4), 774 (2008).
4. D.S. Fudge and J.M. Gosline: Molecular design of the α–keratin composite: Insights from a matrix–free model, hagfish slime threads. *Proc. Biol. Sci.* **271**(1536), 291 (2004).
5. M. Guthold, W. Liu, E. Sparks, L. Jawerth, L. Peng, M. Falvo, R. Superfine, R. Hantgan, and S. Lord: A comparison of the mechanical and structural properties of fibrin fibers with other protein fibers. *Cell Biochem. Biophys.* **49**(3), 165 (2007).
6. J.E. Bertram and J.M. Gosline: Functional design of horse hoof keratin: The modulation of mechanical properties through hydration effects. *J. Exp. Biol.* **130**(1), 121 (1987).
7. J.B. Speakman: 38—the intracellular structure of the wool fibre. *J. Text. Inst., Trans.* **18**(10), T431 (1927).

8. W.T. Astbury and H.J. Woods: X-ray studies of the structure of hair, wool, and related fabrics II. The molecular structure and elastic properties of hair keratin. *Philos. Trans. R. Soc. London* **232**, 333 (1934).
9. W.T. Astbury and A. Street: X-ray studies of the structure of hair, wool, and related fibres I—general. *Philos. Trans. R. Soc. London* **230**, 75 (1932).
10. L. Kreplak, J. Doucet, and F. Briki: Unraveling double stranded alpha-helical coiled coils: An x-ray diffraction study on hard alpha-keratin fibers. *Biopolymers* **58**(5), 526 (2001).
11. L. Kreplak, J. Doucet, P. Dumas, and F. Briki: New aspects of the α-helix to β-sheet transition in stretched hard α-keratin fibers. *Biophys. J.* **87**(1), 640 (2004).
12. J.W.S. Hearle: The structural mechanics of fibers. *J. Polym. Sci., Part C: Polym. Symp.* **20**(1), 215 (1967).
13. J.W.S. Hearle: Chapman mechanical model for wool and other keratin fibers. *Text. Res. J.* **39**(12), 1109 (1969).
14. J.W.S. Hearle: A critical review of the structural mechanics of wool and hair fibres. *Int. J. Biol. Macromol.* **27**(2), 123 (2000).
15. M. Feughelman and A.R. Haly: Structural features of keratin suggested by its mechanical properties. *Biochim. Biophys. Acta* **32**(2), 596 (1959).
16. M. Feughelman: Role of the microfibrils in the mechanical-properties of alpha-keratins. *J. Macromol. Sci. Phys.* **B16**(1), 155 (1979).
17. M. Feughelman: A model for the mechanical-properties of the alpha-keratin cortex. *Text. Res. J.* **64**(4), 236 (1994).
18. M. Feughelman: *Mechanical Properties and Structure of Alpha-Keratin Fibres: Wool, Human Hair and Related Fibres* (UNSW Press, Sydney, Australia, 1997).
19. M. Feughelman: Natural protein fibers. *J. Appl. Polym. Sci.* **83**(3), 489 (2002).
20. F-J. Wortmann and H. Zahn: The stress/strain curve of α-keratin fibers and the structure of the intermediate filament. *Text. Res. J.* **64**(12), 737 (1994).
21. B.M. Chapman and M. Feughelman: Aspects of the structure of α-keratin derived from mechanical properties. *J. Polym. Sci., Part C: Polym. Symp.* **20**(1), 189 (1967).
22. Z. Qin, L. Kreplak, and M.J. Buehler: Hierarchical structure controls nanomechanical properties of vimentin intermediate filaments. *PLoS One* **4**(10), e7294 (2009).
23. Z. Qin and M. Buehler: Structure and dynamics of human vimentin intermediate filament dimer and tetramer in explicit and implicit solvent models. *J. Mol. Model.* **17**(1), 37 (2011).
24. Z. Qin, C-C. Chou, L. Kreplak, and M. Buehler: Structural, mechanical and functional properties of intermediate filaments from the atomistic to the cellular scales. In *Advances in Cell Mechanics*, S. Li and B. Sun, ed.; Springer: Berlin, Heidelberg, 2012; p. 117.
25. C.C. Chou and M.J. Buehler: Structure and mechanical properties of human trichocyte keratin intermediate filament protein. *Biomacromolecules* **13**(11), 3522 (2012).
26. N.G. Azoia, M.M. Fernandes, N.M. Micaêlo, C.M. Soares, and A. Cavaco-Paulo: Molecular modeling of hair keratin/peptide complex: Using MM-PBSA calculations to describe experimental binding results. *Proteins* **80**(5), 1409 (2012).
27. R.L.C. Akkermans and P.B. Warren: Multiscale modelling of human hair. *Philos. Trans. A Math. Phys. Eng. Sci.* **362**(1821), 1783 (2004).
28. T. Ackbarow, D. Sen, C. Thaulow, and M.J. Buehler: Alpha-helical protein networks are self-protective and flaw-tolerant. *PLoS One* **4**(6), e6015 (2009).
29. Z. Qin and M.J. Buehler: Mechanical properties of crosslinks controls failure mechanism of hierarchical intermediate filament networks. *Theor. Appl. Mech. Lett.* **2**(1), 13-014005 (2012).
30. M.J. Buehler: Nature designs tough collagen: Explaining the nanostructure of collagen fibrils. *Proc. Natl. Acad. Sci.* **103**(33), 12285 (2006).
31. M.J. Buehler: Molecular nanomechanics of nascent bone: Fibrillar toughening by mineralization. *Nanotechnology* **18**(29), 295102 (2007).
32. M.J. Buehler: Nanomechanics of collagen fibrils under varying cross-link densities: Atomistic and continuum studies. *J. Mech. Behav. Biomed. Mater.* **1**(1), 59 (2008).
33. T. Ackbarow and M. Buehler: Superelasticity, energy dissipation and strain hardening of vimentin coiled-coil intermediate filaments: Atomistic and continuum studies. *J. Mater. Sci.* **42**(21), 8771 (2007).
34. M.J. Buehler: Hierarchical chemo-nanomechanics of proteins: Entropic elasticity, protein unfolding and molecular fracture. *J. Mech. Mater. Struct.* **2**(6), 1019 (2007).
35. S. Plimpton: Fast parallel algorithms for short-range molecular dynamics. *J. Comput. Phys.* **117**(1), 1 (1995).
36. S. Keten, C.C. Chou, A.C.T. van Duin, and M.J. Buehler: Tunable nanomechanics of protein disulfide bonds in redox microenvironments. *J. Mech. Behav. Biomed. Mater.* **5**(1), 32 (2012).
37. L. Kreplak, A. Franbourg, F. Briki, F. Leroy, D. Dallé, and J. Doucet: A new deformation model of hard α-keratin fibers at the nanometer scale: Implications for hard α-keratin intermediate filament mechanical properties. *Biophys. J.* **82**(4), 2265 (2002).
38. Y. Kajiura, S. Watanabe, T. Itou, K. Nakamura, A. Iida, K. Inoue, N. Yagi, Y. Shinohara, and Y. Amemiya: Structural analysis of human hair single fibres by scanning microbeam SAXS. *J. Struct. Biol.* **155**(3), 438 (2006).
39. H. Zahn: Progress report on hair keratin research. *Int. J. Cosmet. Sci.* **24**(3), 163 (2002).
40. T. Ackbarow and M.J. Buehler: Hierarchical coexistence of universality and diversity controls robustness and multi-functionality in protein materials. *J. Comput. Theor. Nanosci.* **5**(7), 1193 (2008).
41. T. Ackbarow, S. Keten, and M.J. Buehler: A multi-timescale strength model of alpha-helical protein domains. *J. Phys: Condens. Matter* **21**(3), 035111 (2009).
42. A.V. Sokolova, L. Kreplak, T. Wedig, N. Mücke, D.I. Svergun, H. Herrmann, U. Aebi, and S.V. Strelkov: Monitoring intermediate filament assembly by small-angle x-ray scattering reveals the molecular architecture of assembly intermediates. *Proc. Natl. Acad. Sci.* **103**(44), 16206 (2006).
43. Z. Qin, A. Fabre, and M. Buehler: Structure and mechanism of maximum stability of isolated alpha-helical protein domains at a critical length scale. *Eur. Phys. J. E: Soft Matter* **36**(5), 1 (2013).
44. D.A. Greenberg and D.S. Fudge: Regulation of hard α-keratin mechanics via control of intermediate filament hydration: Matrix squeeze revisited. *Proc. Biol. Sci.* **280**(1750), 20122158 (2013).
45. R. Paquin and P. Colomban: Nanomechanics of single keratin fibres: A Raman study of the alpha-helix ->beta-sheet transition and the effect of water. *J. Raman Spectrosc.* **38**(5), 504 (2007).